R. & M. No. 3027
(17,633)
A.R.C. Technical Report

MINISTRY OF SUPPLY

AERONAUTICAL RESEARCH COUNCIL
REPORTS AND MEMORANDA

An Investigation of the Velocity Distribution around the Nose of the Aerofoil with a Flap

By

IAN H. RETTIE,
Engineering Laboratory, Cambridge

Communicated by Prof. W. A. Mair

LONDON: HER MAJESTY'S STATIONERY OFFICE
1957
PRICE 4*s* 6*d* NET

An Investigation of the Velocity Distribution around the Nose of the Aerofoil with a Flap

By

IAN H. RETTIE,

Engineering Laboratory, Cambridge

Communicated by Prof. W. A. Mair

Reports and Memoranda No. 3027

May, 1955

Summary.—The velocity distribution around the nose of an NACA 0015-64 aerofoil was found by experiment and that around the nose of a Piercy 15/40 aerofoil by calculation for various angles of incidence and flap deflection. It was established that at all incidences this velocity distribution is a function of the position of the stagnation point, irrespective of the flap deflection.

This result is shown to be true generally, and it is suggested that use might be made of it in the design of a lift-coefficient meter, which could also be used to give warning of a stall.

1. *Introduction.*—There has been a good deal of interest recently in the direct measurement of lift coefficient in flight and in the prediction of stalling. Several devices have been suggested, of which one of the best known is the American ' safe-flight indicator '. In effect, this gives warning to the pilot of the movement of the stagnation point past a critical position on a cross section of the wing. The claim of the designers that it functions independently of flap angle implies that the stall always occurs with the stagnation point in approximately the same position. This hypothesis is supported by the theoretical work given below, and has also been checked by experiment.

The usual cruise procedure for long-range aircraft involves flying at constant lift coefficient (or incidence). The problem of maintaining the required cruising conditions could therefore be simplified by the use of a meter giving a direct indication of lift coefficient (or incidence). The latter part of this report contains proposals for such a device, suggested by the experimental results, and explains how it could also be used to give warning of a stall.

Previous work of this nature in Britain is limited to a report by G. E. Pringle published in 1941. Measurements of pressure were made at a point on the underside of the nose of a Spitfire wing in flight and an estimation of stalling speed obtained. Satisfactory results were obtained as far as the experiments were pursued and the present paper suggests that a pressure difference between two points on the upper surface of the nose should be used to measure lift coefficient. This arrangement should give better sensitivity and more information. It is established that while the relation between the pressure difference and lift coefficient would change with flap deflection, the value of the pressure difference at which a stall is iminent would not. Hence warning of a stall is obtained for any position of the flap.

2. *Theory.*—The calculation of velocity distributions about aerofoils is generally carried out by the methods given by Theodorsen[2] and by Garrick or by modifications to these methods such as those given by Goldstein[3] and by Thwaites.

In Appendix I the features of Goldstein's work of particular interest to the present problem are summarised. The velocities at the nose and at a neighbouring point on the upper surface of a Piercy 15/40 aerofoil[4] were first calculated in this way for various incidences and deflections of a 20 per cent chord flap. The results are shown in Figs. 9 and 10.

Goldstein's methods do not, however, lend themselves readily to a general investigation of the effects of a deflected flap. Lighthill's hodograph method[5] is more easily applied, and depends upon the fact that $\log q/U$ and γ are conjugate functions with respect to the argument ϕ. They are thus connected by the relation (Poisson's equation) :

$$\log \frac{q}{U}(t) = \frac{1}{2\pi} \int_{-\pi}^{\pi} \gamma(\phi) \cot \frac{t-\phi}{2} \, d\phi \, .$$

Figs. 3 and 4 show the function γ plotted against ϕ and x for a symmetrical aerofoil with an undeflected flap and the front stagnation point at the leading edge. Fig. 5 explains the method of dealing with the deflection of the flap mathematically. The centre-line of the aerofoil for $x > X_\eta$ is supposed to deflect through an angle η but the chord-line is not supposed to alter in relation to the forward part of the aerofoil. The flap is then drawn according to the equation $(x > X_\eta)$:

$$\gamma_\eta = \tan^{-1} \frac{dy_\eta}{dx} = \tan^{-1} \frac{dy}{dx} + \eta = \gamma_0 + \eta$$

and the graph in Fig. 6 is obtained by assuming that the incidence of the aerofoil is altered so that the front stagnation point remains at the leading edge. The rear stagnation point is always taken at the trailing edge of the flap in accordance with Joukowski's hypothesis for the circulation.

This approach differs from Goldstein's, both in the definition of the chord-line and in the construction of the deflected flap, but by keeping the chord-line stationary with respect to the forward part of the aerofoil, while the flap deflects, it avoids the slight distortion of the nose shape involved in Goldstein's method. These differences in shape are not likely to lead to grave discrepancies in the calculated velocity distributions, and from Fig. 7 it may be seen that the difference in chord-line can be allowed for by decreasing the incidence of Goldstein's aerofoil by an amount α_η.

In all theories of wing sections, a transformation is established from the section to a circle. This defines a one-to-one correspondence between the points of the section and of the circle which will be slightly altered when the flap is deflected. In Appendix I it is explained how Goldstein derives a function $\varepsilon_{c\eta}$, which is independent of the section shape and which takes account of this alteration. In Appendix II the problem is approached by Lighthill's method and a similar function ε_η is obtained and identified with Goldstein's $\varepsilon_{c\eta}$. The hodograph method is then developed to estimate the effect of the deflection of the flap on the velocity distribution near the nose of an arbitrary aerofoil. It is found that if the incidence and flap deflection are altered simultaneously, so as to maintain a fixed position of the stagnation point, the velocity distribution near the nose will remain constant, to a first approximation. It is reasonable, to suppose that a nose stall will depend mainly upon this distribution, and it follows that such a stall will take place at the same position of the stagnation point for all values of the flap deflection. The case of a rear stall will be more complicated but even this is likely to be influenced considerably by the pressure gradient at the nose.

3. *Experiment.*—The aerofoil was a symmetrical one of the NACA series (0015–64)[6]. A split flap was used and it was assumed that there would be a correspondence between the effects of split and hinged flaps on the aerodynamic characteristics of an aerofoil. The aerofoil was studied with flap deflections (as defined in Fig. 8) of 0 deg, 5 deg, 10 deg, 15 deg, 20 deg, and 60 deg, and also with the flap removed. The angle of attack was measured relative to the chord of the aerofoil, no account being taken of the flap (*see* Fig. 8).

The chords of the aerofoil and flap were 5 in. and 1·25 in., respectively. The aerofoil was placed in a tunnel whose working-section measured $7\frac{1}{2}$ in. by 20 in. Interference of the tunnel surfaces on the velocity distribution about the aerofoil was therefore fairly small. The wind speed was varied between 40 and 80 feet per second, giving Reynolds numbers between 10^5 and $2{\cdot}0 \times 10^5$. This low value of the Reynolds number would affect the precise nature of the correspondence between the effects of split and hinged flaps referred to above, but this does not matter for the present purpose.

From measurements of pressures at several holes around the nose of the aerofoil, the ratio of the velocity outside the boundary layer, at the positions of the pressure holes to the free-stream velocity, was calculated, for angles of attack up to the stall and each flap angle. The holes were distributed around the nose as follows :—

	Lower surface					Upper surface			
Hole number	4	3	2	1	0	1	2	3	4
x/c	0·0516	0·0258	0·0125	0·00359	0	0·0035	0·0122	0·0260	0·0485
y/c	0·0411	0·0310	0·0227	0·0131	0	0·0125	0·0223	0·0312	0·0402

A nose stall was observed for each flap angle, except at 60 deg when a tail stall occurred. There was, however, a ' bubble separation ' near the nose in this case.

The angles of attack for which the stagnation point was situated exactly at a hole on the lower surface were found, and the position of the stagnation point is plotted in Fig. 12. Fig. 13 shows the difference between the velocity ratios at the first and second holes in the upper surface, plotted against incidence for each flap angle.

4. *Discussion of the Results.*—The most striking feature of the results is the similarity of the ways in which the velocity distributions develop, from the passing of the nose by the stagnation point to the stall. Some typical velocity distributions are shown in Figs. 14 and 15, the latter referring to an incidence just below that at which stalling occurs. It can be seen that the velocity distribution round the nose is a function of the position of the stagnation point, and that stalling occurs when the stagnation point is 3·8 per cent of the chord length from the leading edge. The holes on the upper surface are not closely enough spaced to determine the velocity peaks precisely, but it appears that the maximum value of the velocity ratio, and the position at which this occurs, are constant for a given position of the stagnation point.

The pressure measurements may contain small inaccuracies caused by unsteadiness in the flow. This was as large as 3 per cent at incidences near the stall.

A more precise instance of the similarity of the velocity distributions is the fact that, with only one exception, the stall occurs when the velocity at the first hole along the upper surface becomes greater than that at the second. The difference between the velocity ratios at these two points is plotted in Fig. 13. It varies linearly with incidence and therefore with lift coefficient. It may also be noticed that the lines for each flap angle are parallel. The result was forecast on theoretical grounds (Appendix II), and a system of parallel straight lines was obtained by calculation (Fig. 19) for the velocity ratios at two points on the nose of the Piercy 15/40 aerofoil.

5. *Applications.*—If now the velocity ratios at two holes in the upper surface could be measured in flight, their difference would give an immediate indication of lift coefficient for a chosen flap deflection and of a stall for any flap deflection. This would involve the division of the pressure difference between the holes by the dynamic pressure of the free stream, and could be carried

out by a mechanism similar to that used in a machmeter. The holes to be used on any aerofoil would be on the upper surface near the nose, on either side of the point of maximum velocity (whose position could be found approximately by Goldstein's method). For best results one hole should be on the flat part of the velocity curve behind the maximum. The velocity ratio at this hole will not vary greatly with incidence, while if the other point is very near the position of maximum velocity at the stall, the ratio there will increase rapidly with incidence.

The lift coefficient at a cross-section of a finite wing is directly related to that of the whole wing, and only a simple calibration would be involved. For purposes of stall warning it would be desirable to choose a cross-section near the origin of the stall and for this some experience might be necessary.

6. *Conclusions.*—The velocity distribution around the nose of a given aerofoil is a function of the position of the stagnation point. This has been established for the extreme case of a 25 per cent chord flap at 60 deg and shown theoretically to be true for any aerofoil.

Further, if an aerofoil stalls from the nose, the stall will take place at the same positions both of the stagnation point and of the point of maximum velocity, for all flap deflections.

Use may be made of these facts in the design of a lift-coefficient meter which would also give warning of a stall independently of flap deflection.

NOTATION

c		Chord length of the aerofoil
q		Velocity at a point on the aerofoil
U		Free-stream velocity
x		Distance along the aerofoil chord from the leading edge
X_η		Position of the flap hinge on the aerofoil chord
w		Complex potential function
y		Distance of a point on the aerofoil surface from the chord
z		Circle plane
α		Angle of incidence
β	$=$	$\varepsilon(\pi)$
γ		Angle between the tangent at a point on the aerofoil and the chord
$\varepsilon(\theta)$	$=$	$\phi - \theta$
ζ		Aerofoil plane
η		Flap angle of hinged flap
μ		Flap angle of split flap
θ	$=$	$\cos^{-1}(1 - 2x)$
Θ_η	$=$	$\cos^{-1}(1 - 2X_\eta)$
ϕ		Argument in circle plane
${}_\beta q_\eta$		Value of q for the aerofoil with flap angle η and with the front stagnation point at $\phi = -\beta$

REFERENCES

No.	Author	Title, etc.
1	G. E. Pringle	Stall-warning devices. A.R.C. 5049. 1941.
2	T. Theodorsen	Theory of wing sections of arbitrary shape. N.A.C.A. Report 411. 1931.
3	S. Goldstein	Approximate two-dimensional aerofoil theory. Parts 1—VI. C.P.68 to 73. May, 1942 to August, 1945.
4	C. N. H. Lock and J. H. Preston ..	A new type of aerofoil section. *Aircraft Engineering*. April, 1939.
5	M. J. Lighthill	A new method of two-dimensional aerodynamic design. R. & M. 2112. April, 1945.
6	J. H. Abbott and A. E. von Doenhoff ..	*Theory of Wing Sections*. McGraw-Hill Book Co. 1949.

APPENDIX I

Goldstein[3], following Theodorsen, transforms the aerofoil to the nearly circular curve $z' = a\,e^{\chi+i\theta}$ by means of the transformation :

$$\zeta = z' + \frac{a^2}{z'} \quad .. \quad .. \quad .. \quad .. \quad .. \quad .. \quad .. \quad .. \quad .. \qquad (1)$$

and then to the circle :

$$z = a\,e^{\chi_0+i\phi}$$

by $$z' = z\,e^{\chi-\chi_0+i(\theta-\phi)} \quad .. \quad .. \quad .. \quad .. \quad .. \quad .. \quad .. \quad .. \qquad (2)$$

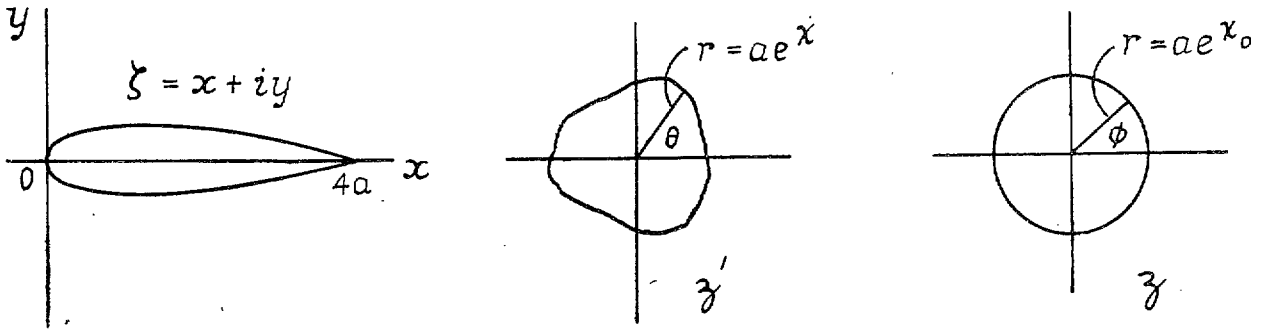

From (1) he deduces the approximate equations (putting $4a = 1$, χ small) :

$$\left.\begin{aligned} x &= \tfrac{1}{2}(1 - \cos\theta) \\ y &= \tfrac{1}{2}\chi \sin\theta \end{aligned}\right\}, \quad .. \quad .. \quad .. \quad .. \quad .. \quad .. \quad .. \qquad (3)$$

and from (2) by Poisson's equation that :

$$\varepsilon(\phi) = \phi - \theta = \frac{1}{2\pi}\int_{-\pi}^{\pi} \chi \cot\frac{\phi - t}{2}\,dt\,. \quad .. \quad .. \quad .. \quad .. \quad .. \qquad (4)$$

Adding the effect of thickness and camber, he puts $y = y_c + y_s$ along the upper surface, and $y = y_c - y_s$ along the lower surface, and from (3) and (4) it is obvious that then $\varepsilon = \varepsilon_c + \varepsilon_s$ along the upper surface, and $\varepsilon = \varepsilon_c - \varepsilon_s$ along the lower surface.

For an aerofoil with a hinged flap put $\varepsilon_c = \varepsilon_{c0} + \varepsilon_{c\eta}$, where $\varepsilon_{c\eta} = 0$ when $\eta = 0$.

Then, the centre-line corresponding to $\varepsilon_c = \varepsilon_{c\eta}$ is (h = chord of flap) :

$$y_c = m_1 x,\ 0 < x < X_\eta, \text{ where } m_1 = \frac{h \sin \eta}{\sqrt{(1 - h^2 \sin^2 \eta)}}$$

$$= m_2(1 - x),\ X_\eta < x < 1, \text{ where } m_2 = \tan (\eta - \tan^{-1} m_1).$$

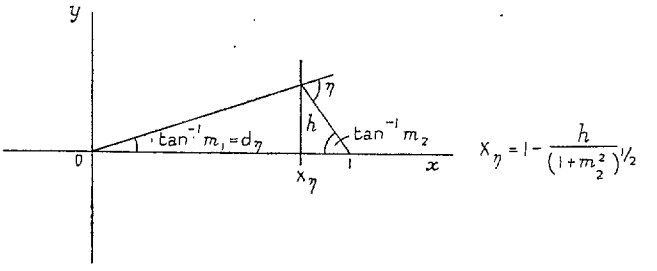

This gives

$$\varepsilon_{c\eta} = -\frac{1}{\pi}\left[m_1 \tan\frac{\theta}{2} - m_2 \cot\frac{\theta}{2}\right] \log_e \frac{\sin \frac{1}{2}(\theta - \Theta_\eta)}{\sin \frac{1}{2}(\theta + \Theta_\eta)} + m_2 - \frac{\Theta_\eta}{\pi}(m_1 + m_2),$$

$$= m_2 - \frac{\Theta_\eta}{\pi}(m_1 + m_2), \text{ when } \theta = \Theta_\eta$$

and this is plotted in Fig. 11 for a 25-per cent chord flap deflected 60 deg.

For the velocity distribution round an aerofoil, Goldstein obtains :—

$$\frac{q}{U} = e^{\chi_0} \frac{(1 - \varepsilon')}{\sqrt{(\chi^2 + \sin^2 \theta)}} \{\sin(\phi + \alpha) + \sin(\alpha + \beta)\}, \text{ where } \beta = \varepsilon(\pi),$$

$$= 0, \text{ when } \phi = -2\alpha - \beta.$$

Thus, if the flap is deflected through an angle η and the stagnation point is at $\phi = \delta$, the incidence of the ' aerofoil chord ' as defined in the text is,

$$\alpha = -\tfrac{1}{2}(-\delta + \varepsilon_s(\pi) + \varepsilon_{c0}(\pi) + \varepsilon_{c\eta}(\pi)) - \alpha_\eta,$$

$$= -\tfrac{1}{2}(-\delta + \beta_0 + \beta_\eta + 2\alpha_\eta), \text{ where } \beta_0 = \varepsilon_s(\pi) + \varepsilon_{c0}(\pi).$$

APPENDIX II

Assume the free-stream velocity at infinity to be unity.

$$\text{Let } \zeta = z + a_1 \log z + \frac{a_2}{z} + \frac{a_3}{z^2} + \ldots\ldots, \text{ say.}$$

Then $$\frac{d\zeta}{dz} = 1 + \frac{b_1}{z} + \frac{b_2}{z^2} + \ldots\ldots.$$

Now $$\frac{dw}{dz} = e^{-i\alpha} - \frac{e^{i\alpha}}{z^2} + \frac{2i \sin \alpha}{z},$$

and hence $$\frac{d\zeta}{dw} = e^{-i\alpha} + \frac{c_1}{z} + \frac{c_2}{z^2} + \ldots\ldots = \frac{1}{q} e^{i\nu},$$

i.e., $$\log \frac{d\zeta}{dw} = -\log q + i\nu \text{ and } -\log q \text{ and } \nu \text{ are conjugate functions in the Fourier sense.}$$

Hence if $z = r\,e^{i\phi}$ Poisson's theorem gives :

$$\log q(t) = \frac{1}{2\pi}\int_{-\pi}^{\pi} \gamma(\phi)\cot\frac{t-\phi}{2}\,d\phi. \qquad \ldots\ \ldots\ \ldots\ \ldots\ \ldots\ \ldots \qquad (1)$$

Now put $x = \frac{1}{2}(1 - \cos\theta)$ and define a function ε such that $\varepsilon(\theta) = \phi - \theta$. When the front stagnation point is at $\phi = -\beta$ (the rear one being always taken at the trailing edge of the flap), for any given aerofoil, ${}_{\beta}\gamma_0 = f_0(\phi)$, say, and if the stagnation point is moved to $\phi = -2\alpha - \beta$,

$$ {}_{2\alpha+\beta}\gamma_0 = f_0(\phi) + g(\phi),$$

where $g(\phi) = 0, \quad -\beta < \phi < 2\pi - 2\alpha - \beta$

$$= \pi, \quad -2\alpha - \beta < \phi < -\beta$$

By (1), $\log {}_{\beta}q_0(t) = \dfrac{1}{2\pi}\displaystyle\int_{-\pi}^{\pi} f_0(\phi)\cot\frac{t-\phi}{2}\,d\phi,$

and hence

$$\log_{2\alpha+\beta}q_0\,(t) = \log {}_{\beta}q_0\,(t) + \frac{1}{2\pi}\int_{-2\alpha-\beta}^{-\beta} \pi\cot\frac{t-\phi}{2}\,d\phi\,,$$

$$= \log {}_{\beta}q_0\,(t) - \int_{-\alpha-\frac{t}{2}-\frac{\beta}{2}}^{-\frac{t}{2}-\frac{\beta}{2}} \cot u\,du, \text{ where } u = \frac{\phi - t}{2}\,,$$

$$= \log_{\beta}q_0\,(t) + \log\left|\frac{\sin\left(\alpha + \frac{t}{2} + \frac{\beta}{2}\right)}{\sin\left(\frac{t}{2} + \frac{\beta}{2}\right)}\right|.$$

Therefore

$$\frac{{}_{2\alpha+\beta}q_0\,(\phi)}{{}_{\beta}q_0\,(\phi)} = \frac{\sin\frac{1}{2}(2\alpha + \phi + \beta)}{\sin\frac{1}{2}(\phi + \beta)} = \frac{\sin(\phi + \alpha) + \sin(\alpha + \beta)}{\sin\phi + \sin\beta}. \qquad \ldots\ \ldots\ \ldots \qquad (2)$$

This is a well-known result (Appendix I) and is merely an example of the method which will be applied to the case of an aerofoil with a hinged flap.

It is assumed that the deflection of a hinged flap is equivalent to a change in the camber-line of the aerofoil, and that deflection of the flap through an angle η merely decreases by an amount η the inclination to the aerofoil chord of the part of the surface behind the point X_η. For simplicity the chord-line is not varied with η, but the ' aerofoil chord ' is defined as the line joining the leading and trailing edges at $\eta = 0$. The angle of incidence of the aerofoil is the angle between the aerofoil chord and the direction of flow at infinity.

Then for a flap deflection of η, ε_η and $f_\eta(\phi)$ may be defined so that $\phi_\eta - \theta = \varepsilon_0 + \varepsilon_\eta$ where $\varepsilon_\eta \equiv 0$ for $\eta = 0$, and ${}_{\beta-\varepsilon_\eta}\gamma_\eta = f_\eta(\phi)$, with the stagnation point at $\theta = -\beta - \varepsilon_0$.

Now, by Riemann's theorem, conformal transformation is unique. Hence Goldstein's $\varepsilon_{c\eta}$ (Appendix I) may be identified as an approximation to ε_η above. $\varepsilon_{c\eta}$ is plotted in Fig. 11 for a 25-per cent flap deflected 60 deg and it is supposed that since $d\varepsilon_{c_\eta}/d\theta$ is small near the nose, so also will be $d\varepsilon_\eta/d\theta$.

Graphs of ${}_0\gamma_0$ and ${}_{-\varepsilon_\eta}\gamma_\eta$ against ϕ would look something like :

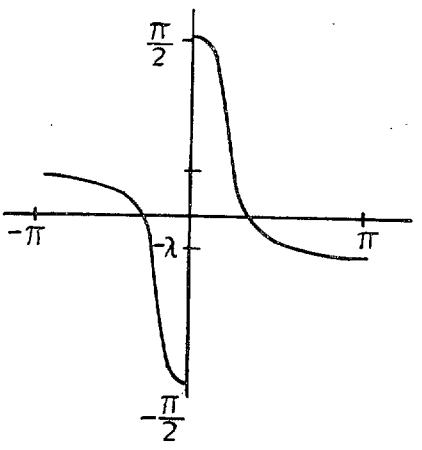

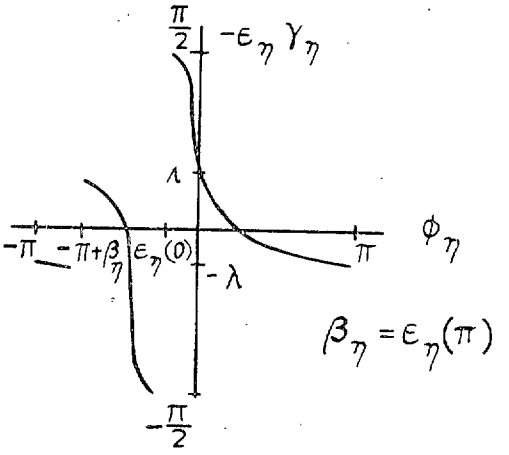

for a symmetrical wing with a trailing-edge angle of 2λ.

It can be seen that $f_0(\phi) = f_\eta(\phi + \varepsilon_\eta)$ and since ε_η is small :

$$f_\eta(\phi) \simeq f_0(\phi - \varepsilon_\eta). \qquad \ldots\ldots\ldots\ldots\ldots\ldots\ldots \tag{3}$$

Let the points $\pm\ \Theta_\eta$ in the upper and lower surfaces of the aerofoil with deflected flap correspond to $\Phi_{\eta u}$ and $-\ \Phi_{\eta l}$ respectively in the circle $|z| = \text{const}$. Now put :

$${}_{2\alpha+\beta-\varepsilon_\eta}\gamma_\eta = f_\eta(\phi) + g(\phi) + h(\phi) \qquad \ldots\ldots\ldots\ldots\ldots\ldots\ldots \tag{4}$$

where
$$g(\phi) = 0, \quad -\beta + \varepsilon_\eta < \phi < 2\pi - 2\alpha - \beta + \varepsilon_\eta$$
$$= \pi, \quad -2\alpha - \beta + \varepsilon_\eta < \phi < -\beta + \varepsilon_\eta,$$

and
$$h(\phi) = 0, \quad -\Phi_{\eta l} < \phi < \Phi_{\eta u}$$
$$= -\eta, \quad -\Phi_{\eta u} < \phi < 2\pi - \Phi_{\eta l}.$$

Now,

$$\frac{1}{2\pi}\int_{-\pi}^{\pi} h(\phi)\cot\frac{t-\phi}{2}\,d\phi = \frac{\eta}{2\pi}\int_{\frac{1}{2}(\Phi_{\eta u}-t)}^{\frac{1}{2}(2\pi-\Phi_{\eta l}-t)} \cot u\,du,$$

$$= \log\left|\frac{\sin\frac{1}{2}(\Phi_{\eta l}+t)}{\sin\frac{1}{2}(\Phi_{\eta u}-t)}\right|^{\frac{\eta}{2\pi}},$$

$$\simeq \log\left|\frac{\sin\frac{1}{2}\Phi_{\eta l} + \frac{1}{2}t\cos\frac{1}{2}\Phi_{\eta l}}{\sin\frac{1}{2}\Phi_{\eta u} - \frac{1}{2}t\cos\frac{1}{2}\Phi_{\eta u}}\right|^{\frac{\eta}{2\pi}}, \ t \text{ small},$$

$$= \log\left(\frac{1+\frac{t}{2}\cot\frac{1}{2}\Phi_{\eta l}}{1-\frac{t}{2}\cot\frac{1}{2}\Phi_{\eta u}}\right)^{\frac{\eta}{2\pi}}\left(\frac{\sin\frac{1}{2}\Phi_{\eta l}}{\sin\frac{1}{2}\Phi_{\eta u}}\right)^{\frac{\eta}{2\pi}},$$

$$= \log A + \log B$$

where $$A = \left(1 + \frac{t}{2}\cot\tfrac{1}{2}\Phi_{\eta l}\right)^{\frac{\eta}{2\pi}}\left(1 + \frac{t}{2}\cot\tfrac{1}{2}\Phi_{\eta u} + \frac{t^2}{4}\cot^2\tfrac{1}{2}\Phi_{\eta u} + \ldots\ldots\right)^{\frac{\eta}{2\pi}}$$

$$= 1 + \frac{\eta}{2\pi}\, t\, \tfrac{1}{2}(\cot\tfrac{1}{2}\Phi_{\eta l} + \cot\tfrac{1}{2}\Phi_{\eta u}) + \ldots\ldots,$$

and $$B = 1 - \frac{\eta}{2\pi}\,\tfrac{1}{2}(\Phi_{\eta u} - \Phi_{\eta l})\cot\tfrac{1}{2}\Phi_{\eta u} + \ldots\ldots.$$

Now $\eta/2\pi$ is small and so also are the cotangents, since $\frac{1}{2}\pi < (\Phi_{\eta l}, \Phi_{\eta u}) < \pi$. Further, by Appendix I, $\frac{1}{2}(\Phi_{\eta u} - \Phi_{\eta l}) \doteq \varepsilon_{c0} + \varepsilon_{c\eta}(\Theta_\eta)$,

and this will in general be small and positive. Hence near the nose when t is small A and B will be very close to unity and on opposite sides of it.

Hence, $$\frac{1}{2\pi}\int_{-\pi}^{\pi} h(\phi)\cot\frac{t-\phi}{2}\,d\phi \doteq 0, \text{ when } t \text{ is small.} \quad \ldots \quad \ldots \quad \ldots \quad (5)$$

Also $$\frac{1}{2\pi}\int_{-\pi}^{\pi} f_\eta(\phi)\cot\frac{t-\phi}{2}\,d\phi = \frac{1}{2\pi}\int_{-\pi}^{\pi} f_0(\phi - \varepsilon_\eta)\cot\frac{t-\phi}{2}\,d\phi, \text{ by equation (3),}$$

$$= \frac{1}{2\pi}\int_{-\pi}^{\pi} f_0(\phi - \varepsilon_\eta + \varepsilon_\eta(0))\cot\frac{t - \varepsilon_\eta(0) - \phi}{2}\,d\phi,$$

$$= \frac{1}{2\pi}\int_{-\pi}^{\pi}\left\{f_0(\phi) + (\varepsilon_\eta(0) - \varepsilon_\eta)\frac{df_0}{d\phi}\right\}\cot\frac{t - \varepsilon_\eta(0) - \phi}{2}\,d\phi.$$

Near the nose $|\varepsilon_\eta(0) - \varepsilon_\eta|$ is very small (*see* Fig. 11) and elsewhere $|\varepsilon_\eta(0) - \varepsilon_\eta|$ and $\left|\cot\frac{t - \varepsilon_\eta(0) - \phi}{2}\right|$ are small if t lies near the nose while $(df_0/d\phi) = (d\gamma/dx)(dx/d\theta)(d\theta/d\phi)$, $= (1/R)\sin 2\theta\{1 + (d\varepsilon/d\phi)\}$, where R is the radius of curvature of the aerofoil surface.

This also is small and so :

$$\frac{1}{2\pi}\int_{-\pi}^{\pi} f_\eta(\phi)\cot\frac{t-\phi}{2}\,d\phi \doteq \frac{1}{2\pi}\int_{-\pi}^{\pi} f_0(\phi)\cot\frac{t - \varepsilon_\eta(0) - \phi}{2}\,d\phi,$$

$$= \log {}_\beta q_0\,(t - \varepsilon_\eta(0)) \quad \ldots \quad \ldots \quad \ldots \quad \ldots \quad \ldots \quad \ldots \quad \ldots \quad (6)$$

Hence by equations (1), (3), (4), (5) and (6) using a method similar to that in the derivation of equation (2) :

$$\log {}_{2\alpha+\beta-\varepsilon_\eta}q_\eta\,(t) \doteq \log {}_\beta q_0\,\{t - \varepsilon_\eta(0)\} + \log\frac{\sin\frac{1}{2}\{t + \beta - \varepsilon_\eta(0) + 2\alpha\}}{\sin\frac{1}{2}\{t + \beta - \varepsilon_\eta(0)\}},$$

$$= \log {}_\beta q_0\,\{t - \varepsilon_\eta(0)\} + \log\frac{\sin\{t - \varepsilon_\eta(0) + \alpha\} + \sin(\alpha + \beta)}{\sin\{t - \varepsilon_\eta(0)\} + \sin\beta}$$

$$= \log_{2\alpha+\beta}q_0\{t - \varepsilon_\eta(0)\}.$$

Now let the points $\theta = \theta_1$ in the aerofoil with undeflected flap and $\theta = \theta_2$ on the aerofoil with deflected flap correspond to the points $\phi = t - \varepsilon_\eta(0)$ and $\phi_\eta = t$ respectively on $|\eta| = \text{const.}$

Then $\log {}_{2\alpha+\beta-\varepsilon_\eta}q_\eta\,(t) = \log {}_{2\alpha+\beta-\varepsilon_\eta}q_\eta\,(\theta_2)$,

and $\log {}_{2\alpha+\beta}q_0\,\{t - \varepsilon_\eta(0)\} = \log {}_{2\alpha+\beta}q_0\,(\theta_1)$.

Also $t - \theta_1 = \varepsilon_0 + \varepsilon_\eta \doteq \varepsilon_0 + \varepsilon_\eta(0)$,

and $t - \varepsilon_\eta(0) - \theta_2 = \varepsilon_0$.

Hence $\theta_1 = \theta_2$.

Further, the stagnation-point positions are $\phi_\eta = -2\alpha - \beta + \varepsilon_\eta$ in the case of the deflected flap and $\phi = -2\alpha - \beta$ in the case of the undeflected flap corresponding to $\theta = -2\alpha - \beta - \varepsilon_0$ in each case.

It has therefore been shown true that for a given position of the stagnation point and for any flap deflection, the velocity distribution around the nose is constant, with the position of the point of maximum velocity (if this is near the leading edge) and the magnitude of the maximum velocity the same to a first approximation. Now it is the velocity distribution around the nose that determines a nose stall, and such a stall will therefore take place with the stagnation point in the same position for all flap deflections.

At the point θ, with incidence α,

$$\begin{aligned} {}_{2\alpha+\beta}q_0\,(\theta) &= C\,\{\sin(\phi + \alpha) + \sin(\alpha + \beta)\}, \\ &\doteq C\,\{\sin\phi + \sin\beta + \alpha(\cos\phi + \cos\beta)\}, \\ &= D + E\alpha \\ &= {}_{2\alpha+\beta+\varepsilon_\eta(0)}q_\eta\,(\theta), \end{aligned}$$

where the incidence is now (Appendix I), $\alpha + \alpha' = \alpha + \frac{1}{2}\varepsilon_\eta(0) - \frac{1}{2}\beta_\eta - \alpha_\eta$.

Hence for incidence α:

$$\begin{aligned} {}_{2(\alpha-\alpha')+\beta+\varepsilon_\eta(0)}q_\eta\,(\theta) &= B + C(\alpha - \alpha'), \\ &= (B - C\alpha') + C\alpha = (B + C\alpha) - C\alpha', \end{aligned}$$

and so if the velocity at a point near the nose is plotted against incidence (measured relative to the aerofoil chord) a family of straight lines, each pertaining to one value of η, is obtained.

It is interesting to note also that α_η, β_η and $\varepsilon_\eta(0)$ are linear with η and hence so is α' (Fig. 11). Thus in Fig. 9 there are two families of parallel straight lines, one for particular values of η and the other for particular values of α.

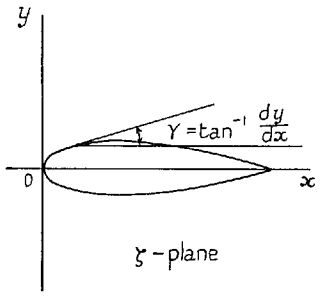

FIG. 1.

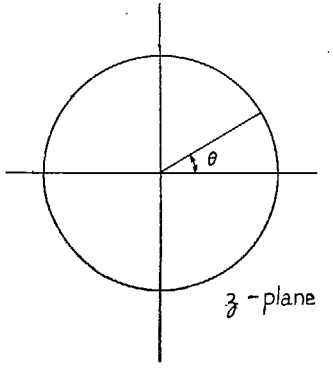

FIG. 2.

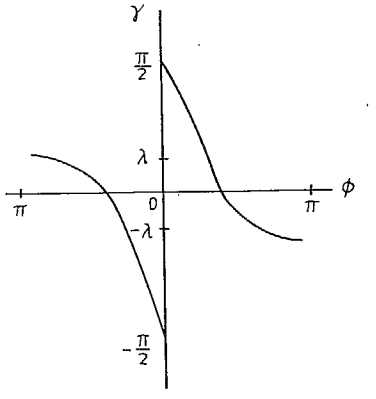

FIG. 3.

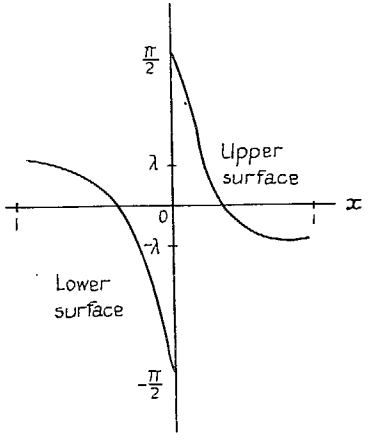

FIG. 4.

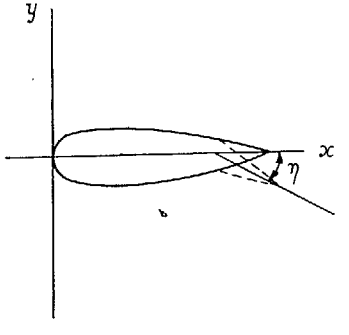

FIG. 5.

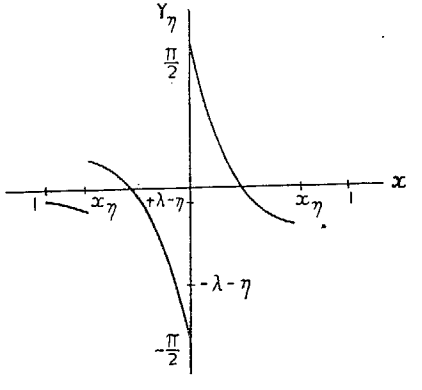

FIG. 6.

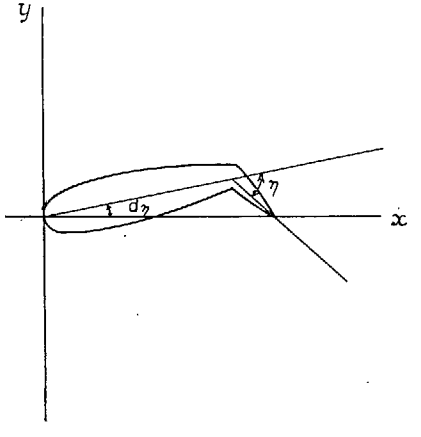

FIG. 7.

FIG. 8.

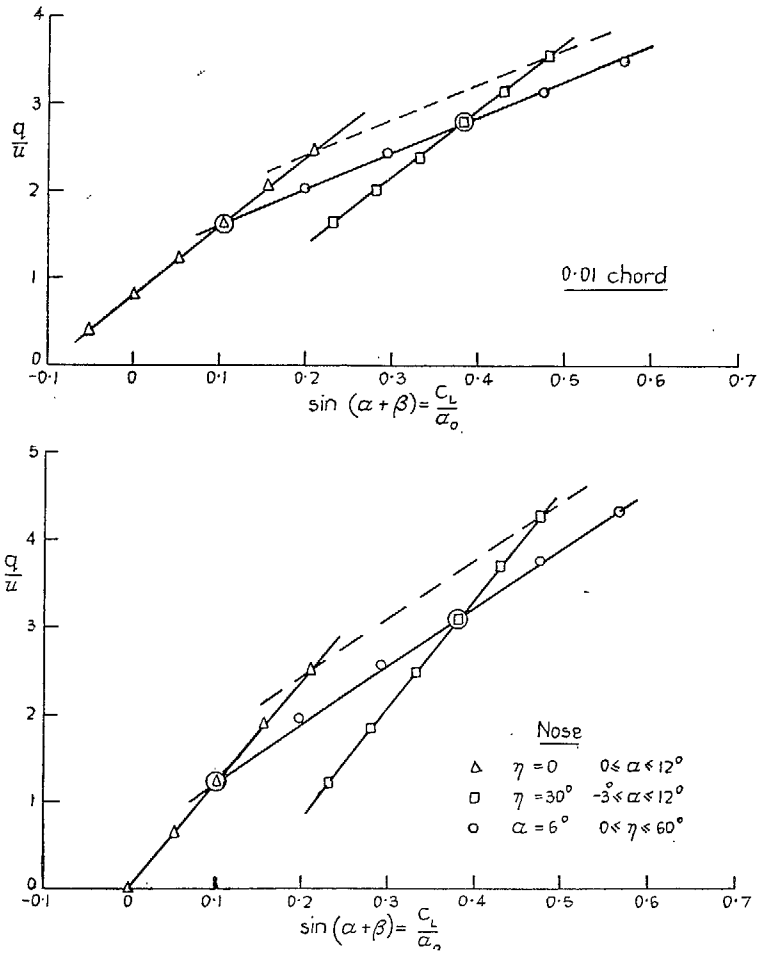

Velocity, at nose and at 0·01 x chord on upper surface, v. lift coefficient. Chord of flap = 0·2 x (chord of wing). α = incidence. η = flap deflection.

FIG. 9. Piercy 15/40 aerofoil.

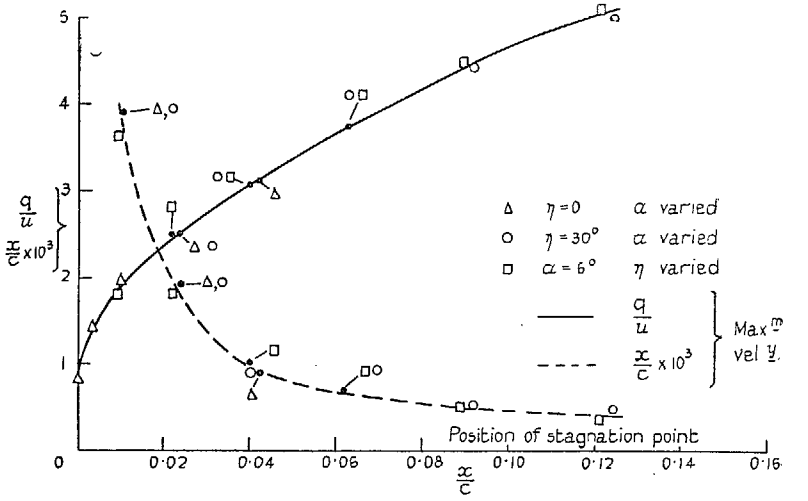

Position and value of maximum upper surface velocity v position of stagnation point

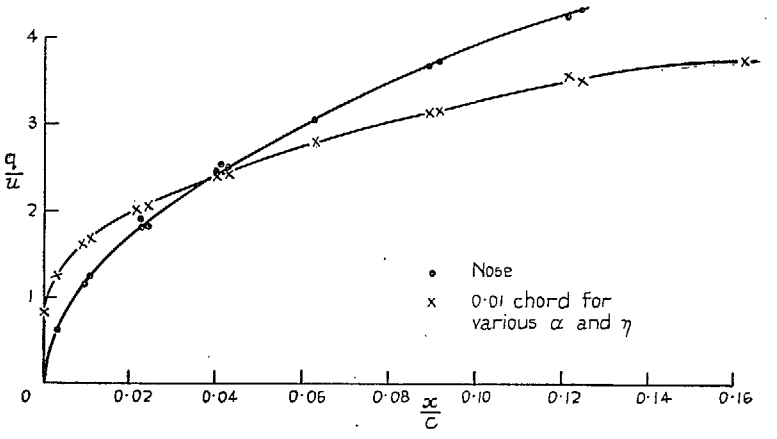

Velocity $\frac{q}{u}$, at nose and 0·01 x chord on upper surface, v. position of stagnation point $\frac{x}{c}$

FIG. 10. Piercy 15/40 aerofoil.

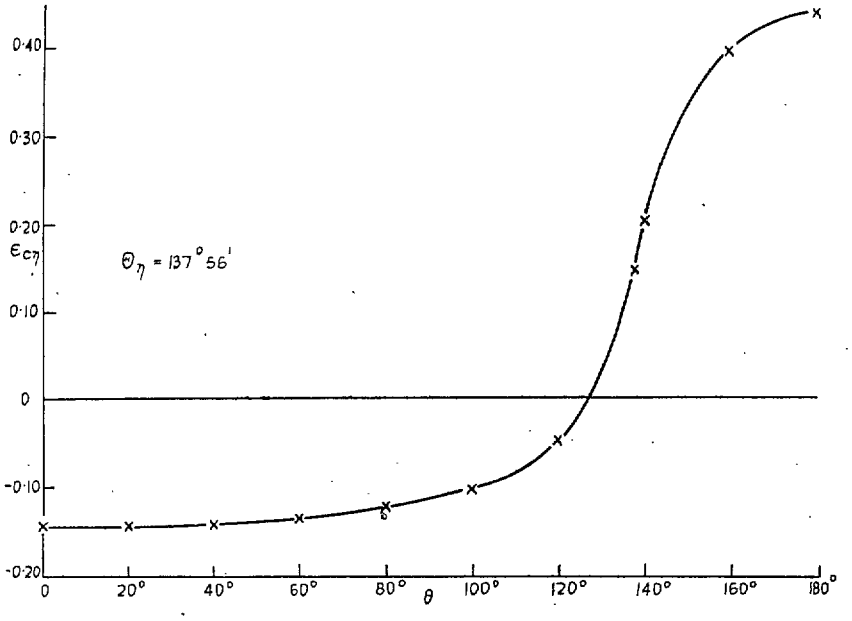

$\epsilon_{c\eta}$ (Goldstein) for a 20% chord flap deflected 60° v. θ.

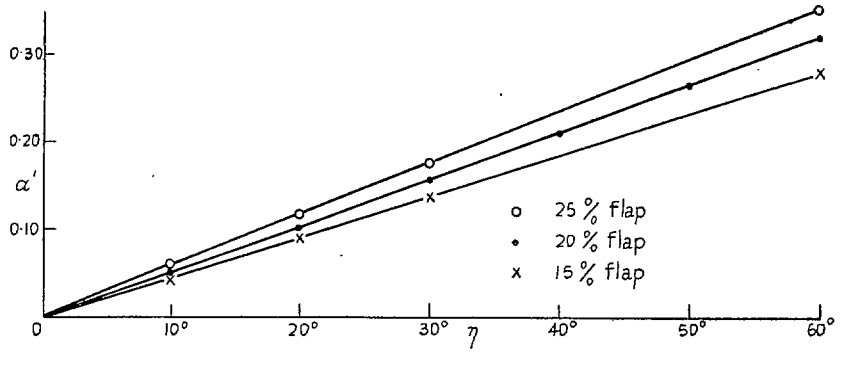

Change of incidence α' required to maintain the position of the stagnation point when the flap is deflected from 0 to η.

FIG. 11. Parameters for hinged flaps.

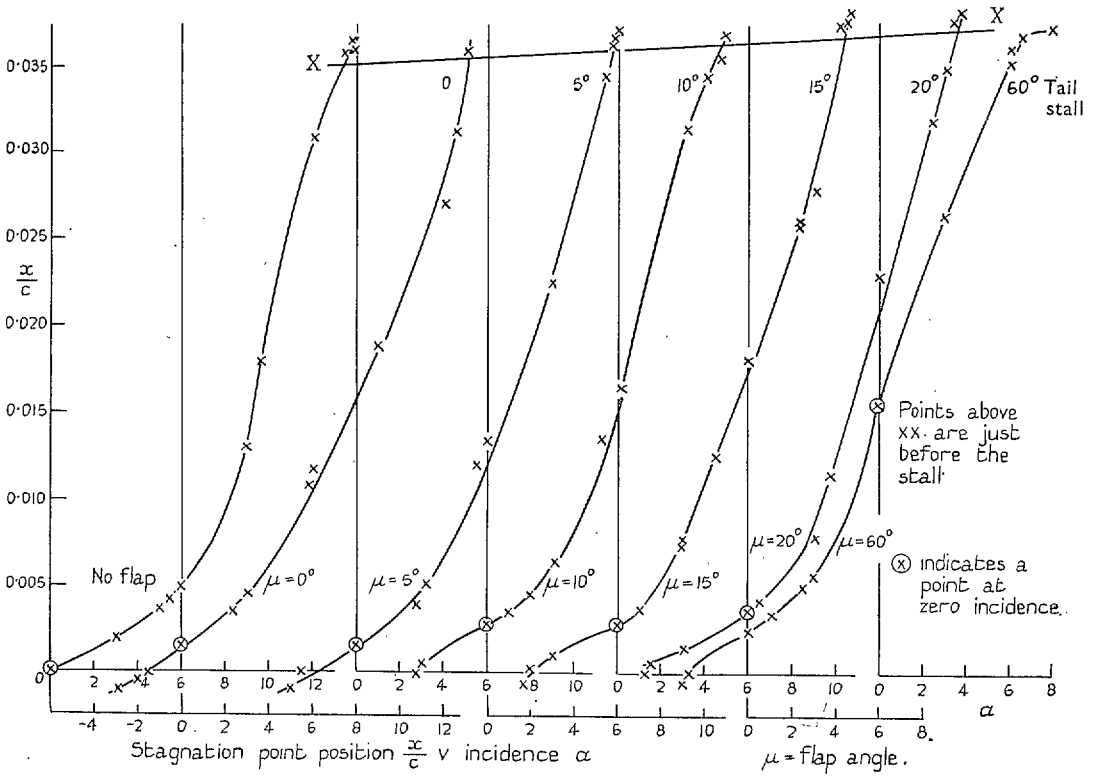

FIG. 12. N.A.C.A. 0015-64 aerofoil.

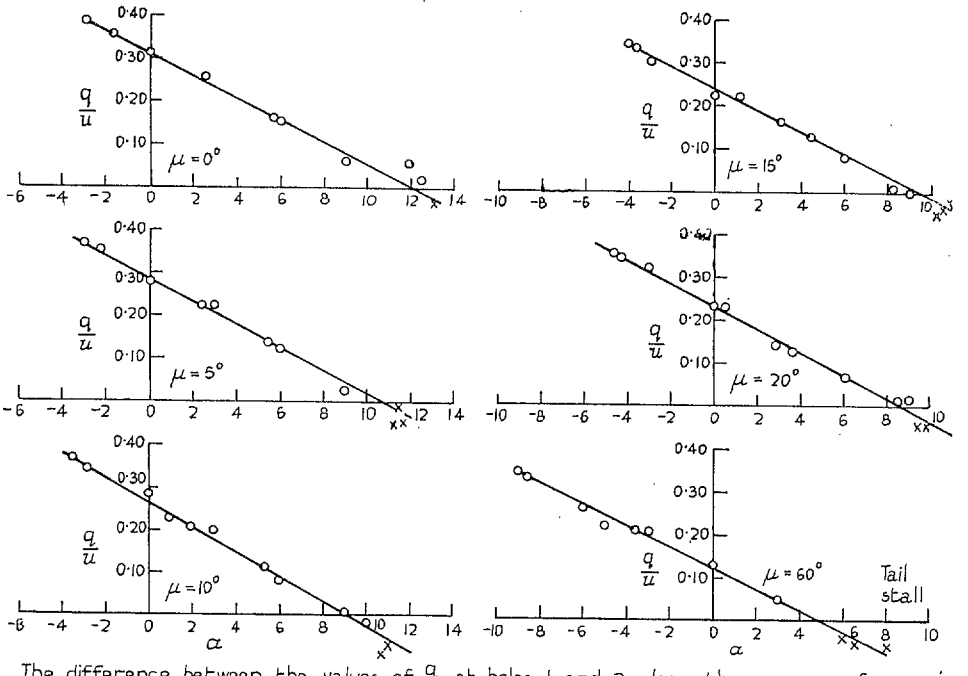

The difference between the values of $\frac{q}{u}$ at holes 1 and 2 along the upper surface v incidence

Crosses represent points just before the stall

FIG. 13. N.A.C.A. 0015-64 aerofoil.

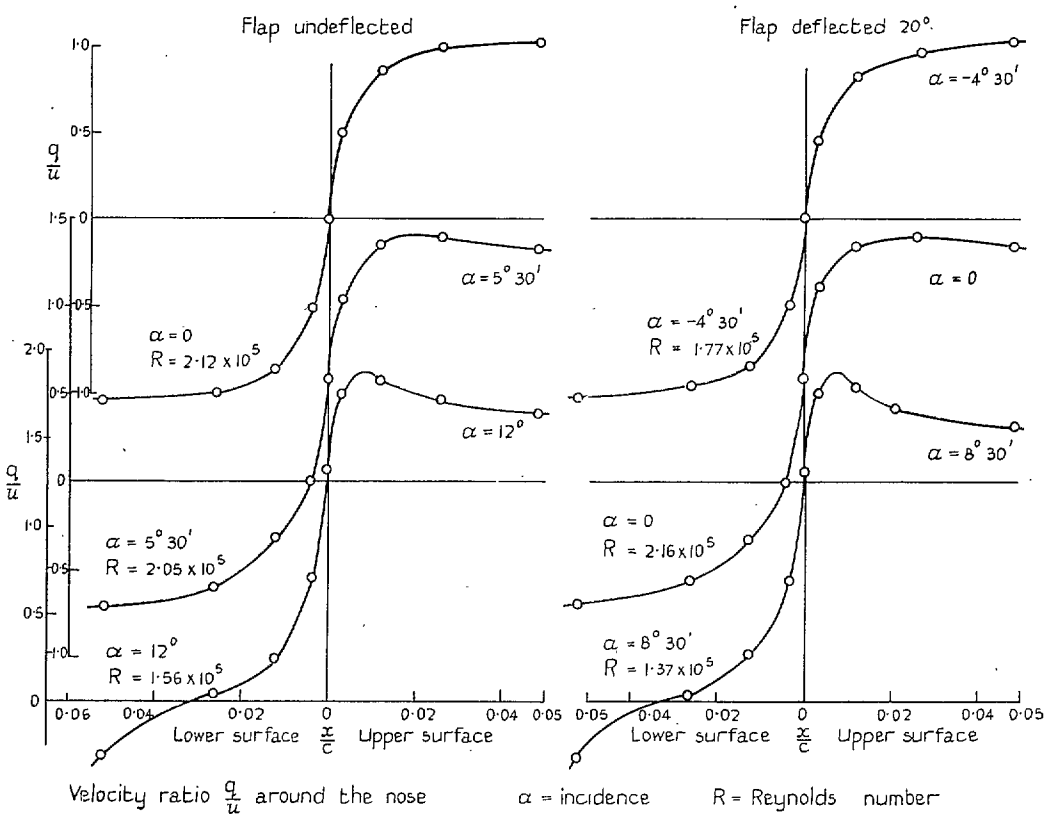

FIG. 14. N.A.C.A. 0015-64 aerofoil.

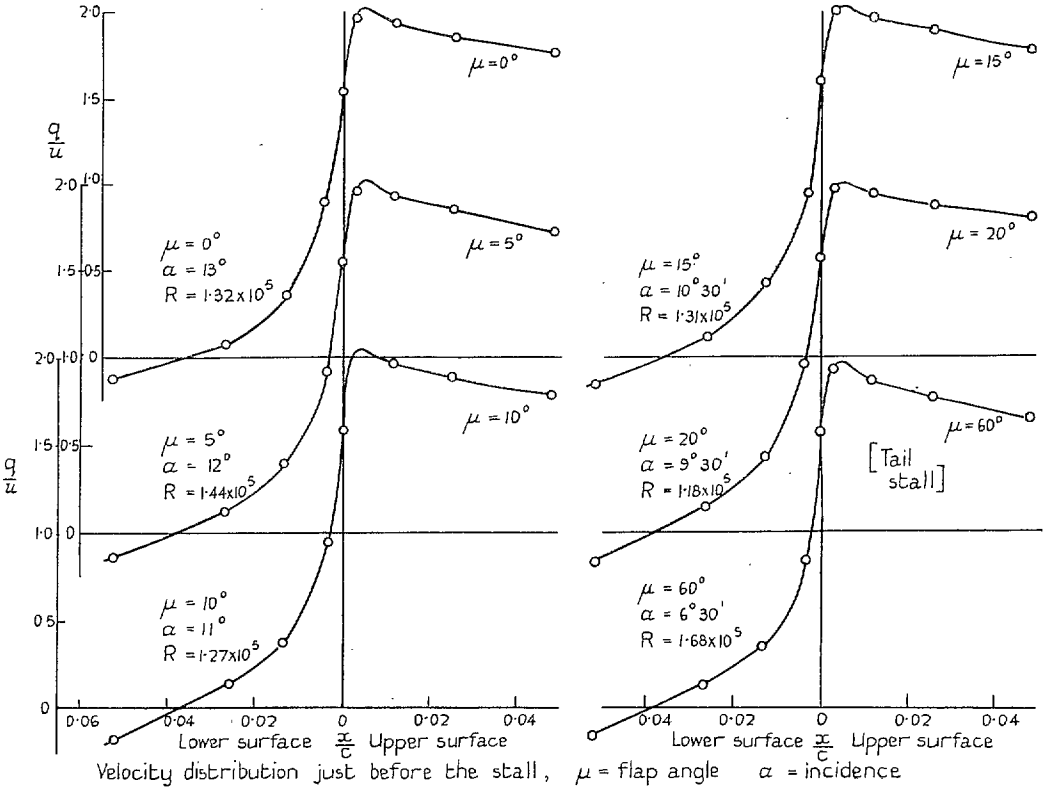

FIG. 15. N.A.C.A. 0015-64 aerofoil.

J4378 Wt.20/9036 K9 11/56 D&Co. 34/263 PRINTED IN GREAT BRITAIN

Publications of the Aeronautical Research Council

ANNUAL TECHNICAL REPORTS OF THE AERONAUTICAL RESEARCH COUNCIL (BOUND VOLUMES)

1939 Vol. I. Aerodynamics General, Performance, Airscrews, Engines. 50*s*. (51*s*. 9*d*.)
Vol. II. Stability and Control, Flutter and Vibration, Instruments, Structures, Seaplanes, etc. 63*s*. (64*s*. 9*d*.)

1940 Aero and Hydrodynamics, Aerofoils, Airscrews, Engines, Flutter, Icing, Stability and Control, Structures, and a miscellaneous section. 50*s*. (51*s*. 9*d*.)

1941 Aero and Hydrodynamics, Aerofoils, Airscrews, Engines, Flutter, Stability and Control, Structures. 63*s*. (64*s*. 9*d*.)

1942 Vol. I. Aero and Hydrodynamics, Aerofoils, Airscrews, Engines. 75*s*. (76*s*. 9*d*.)
Vol. II. Noise, Parachutes, Stability and Control, Structures, Vibration, Wind Tunnels. 47*s*. 6*d*. (49*s*. 3*d*.)

1943 Vol. I. Aerodynamics, Aerofoils, Airscrews. 80*s*. (81*s*. 9*d*.)
Vol. II. Engines, Flutter, Materials, Parachutes, Performance, Stability and Control, Structures. 90*s*. (92*s*. 6*d*.)

1944 Vol. I. Aero and Hydrodynamics, Aerofoils, Aircraft, Airscrews, Controls. 84*s*. (86*s*. 3*d*.)
Vol. II. Flutter and Vibration, Materials, Miscellaneous, Navigation, Parachutes, Performance, Plates and Panels, Stability, Structures, Test Equipment, Wind Tunnels. 84*s*. (86*s*. 3*d*.)

1945 Vol. I. Aero and Hydrodynamics, Aerofoils. 130*s*. (132*s*. 6*d*.)
Vol. II. Aircraft, Airscrews, Controls. 130*s*. (132*s*. 6*d*.)
Vol. III. Flutter and Vibration, Instruments, Miscellaneous, Parachutes, Plates and Panels, Propulsion. 130*s* (132*s*. 3*d*.)
Vol. IV. Stability, Structures, Wind tunnels, Wind Tunnel Technique. 130*s*. (132*s*. 3*d*.)

ANNUAL REPORTS OF THE AERONAUTICAL RESEARCH COUNCIL—

1937 2*s*. (2*s*. 2*d*.) 1938 1*s*. 6*d*. (1*s*. 8*d*.) 1939–48 3*s*. (3*s*. 3*d*.)

INDEX TO ALL REPORTS AND MEMORANDA PUBLISHED IN THE ANNUAL TECHNICAL REPORTS, AND SEPARATELY—

April, 1950 – – – – – R. & M. No. 2600. 2*s*. 6*d*. (2*s*. 8*d*.)

AUTHOR INDEX TO ALL REPORTS AND MEMORANDA OF THE AERONAUTICAL RESEARCH COUNCIL—

1909–January, 1954 – – – R. & M. No. 2570. 15*s*. (15*s*. 6*d*.)

INDEXES TO THE TECHNICAL REPORTS OF THE AERONAUTICAL RESEARCH COUNCIL—

December 1, 1936 — June 30, 1939. R. & M. No. 1850. 1*s*. 3*d*. (1*s*. 5*d*.)
July 1, 1939 — June 30, 1945. – R. & M. No. 1950. 1*s*. (1*s*. 2*d*.)
July 1, 1945 — June 30, 1946. – R. & M. No. 2050. 1*s*. (1*s*. 2*d*.)
July 1, 1946 — December 31, 1946. R. & M. No. 2150. 1*s*. 3*d*. (1*s*. 5*d*.)
January 1, 1947 — June 30, 1947. – R. & M. No. 2250. 1*s*. 3*d*. (1*s*. 5*d*.)

PUBLISHED REPORTS AND MEMORANDA OF THE AERONAUTICAL RESEARCH COUNCIL—

Between Nos. 2251–2349. – – R. & M. No. 2350. 1*s*. 9*d*. (1*s*. 11*d*.)
Between Nos. 2351–2449. – – R. & M. No. 2450. 2*s*. (2*s*. 2*d*.)
Between Nos. 2451–2549. – – R. & M. No. 2550. 2*s*. 6*d*. (2*s*. 8*d*.)
Between Nos. 2551–2649. – – R. & M. No. 2650. 2*s*. 6*d*. (2*s*. 8*d*.)

Prices in brackets include postage

HER MAJESTY'S STATIONERY OFFICE

York House, Kingsway, London W.C.2; 423 Oxford Street, London W.1;
13a Castle Street, Edinburgh 2; 39 King Street, Manchester 2; 2 Edmund Street, Birmingham 3; 109 St. Mary Street, Cardiff; Tower Lane, Bristol 1; 80 Chichester Street, Belfast, *or through any bookseller*

S.O. Code No. 23-3027